nature materials

LETTERS

https://doi.org/10.1038/s41563-019-0281-z

Emergence of quantum correlations from interacting fibre-cavity polaritons

Guillermo Muñoz-Matutano[1,2,7*], Andrew Wood[1,2,7], Mattias Johnsson[1,2,7], Xavier Vidal[1,2], Ben Q. Baragiola[1,2,3], Andreas Reinhard[1,2], Aristide Lemaître[4], Jacqueline Bloch[4], Alberto Amo[5], Gilles Nogues[6], Benjamin Besga[1,2,6], Maxime Richard[1,6] and Thomas Volz[1,2*]

Over the past decade, exciton-polaritons in semiconductor microcavities have revealed themselves as one of the richest realizations of a light-based quantum fluid[1], subject to fascinating new physics and potential applications[2–6]. For instance, in the regime of large two-body interactions, polaritons can be used to manipulate the quantum properties of a light field[7–9]. In this work, we report on the emergence of quantum correlations in laser light transmitted through a fibre-cavity polariton system. We observe a dispersive shape of the autocorrelation function around the polariton resonance that indicates the onset of this regime. The weak amplitude of these correlations indicates a state that still remains far from a low-photon-number state. Nonetheless, given the underlying physical mechanism[7], our work opens up the prospect of eventually using polaritons to turn laser light into single photons.

Exciton-polaritons are hybrid excitations that are partly photonic and partly excitonic in nature, and are present in semiconductor microcavities in the strong coupling regime. To a good approximation, at low density these excitations can be considered to be bosonic as in an ideal harmonic oscillator. At higher densities this description partially breaks down due to Coulomb interactions between polaritons, mediated by their excitonic fraction. This two-body interaction leads to a Kerr-like nonlinearity of the polaritonic state that can be exploited for applications such as parametric down-conversion[10], squeezing[8] and optical spin switches[11]. On increasing the lateral confinement of the polaritonic state, this interaction can be further increased, up to the point where it becomes significant at the level of a few quanta of the polariton field. In this regime, a polariton mode turns into a nonlinear 'quantum filter' that, depending on the input photon statistics (typically a laser beam), can create non-trivial quantum correlations in the output light[7]. Figure 1a shows the low-energy excitation ladder of a polariton state subject to such a strong nonlinearity and illustrates the underlying 'filter' mechanism: once a polariton has been excited by a photon from the incoming beam, the energy required to create a second polariton is larger by a quantity U, the polariton–polariton interaction energy. In other words, the two-polariton state is blueshifted compared to the one-polariton state. Hence, if the laser is resonant or slightly red-detuned with respect to the transition between zero and one polariton, the likelihood of creating two polaritons within a time window comparable with the polariton lifetime is reduced, and the laser light transmitted through the system exhibits antibunching (red arrows in Fig. 1a). This implies that the experimentally measurable second-order autocorrelation function at zero time delay, $g^{(2)}(0)$, drops below 1. Conversely, when the laser is tuned to the blue side of the transition between zero and one polariton, the probability of creating two polaritons at a time is enhanced, resulting in photon bunching in transmission (blue arrows in Fig. 1a). As a result, $g^{(2)}(0)$ exhibits a characteristic dispersive shape as a function of laser detuning as displayed in Fig. 1b. In the limit where U clearly exceeds the polariton linewidth, γ_{LP}, this effect has been termed polariton blockade[7] and is reminiscent of the photon blockade effect in cavity quantum electrodynamics[12,13] and of the Rydberg blockade effect in atomic ensembles[14,15]. In semiconductor systems, photon blockade has been realized for quantum-dot devices[16,17], but achieving polariton blockade would enable a novel class of photonic dots[7] with similar nonlinearity, faster emission rate and an inherent scalability due to the fully deterministic fabrication methods available for photonic nanostructures.

In this work, we observe the build-up of quantum correlations in laser light transmitted through a fibre-cavity polariton system, indicating the onset of this strong interaction regime. As a function of detuning $\Delta_{LP} = E_L - E_{LP}$ (where E_L is the laser energy and E_{LP} is the polaritonic resonance), we observe the characteristic dispersive shape of $g^{(2)}(0; \Delta_{LP})$ caused by strong polariton–polariton interactions. Using a quantitative analysis of this shape based on a master equation approach[7], we are able to match theory and experiment. Our experimental analysis also reveals different sources of noise that partially spoil the fragile photon correlations created by polariton–polariton interactions, namely the charged exciton transition, and the neighbouring fundamental cross-polarized polariton mode. By tuning the system parameters appropriately we show that these perturbations can be minimized. From such a measurement we quantitatively estimate $\hbar g$, the strength of the polariton–polariton nonlinearity. Determining $\hbar g$ has proved a challenging task so far, mainly due to the fact that polaritons are often mixed up with a bare exciton reservoir that contributes to the interactions[18], or to the difficulty of accurately determining the polariton density. We infer $\hbar g$ from the measured $g^{(2)}(0; \Delta_{LP})$, and need the polariton (cavity) mode area as the only additional input. Note that as long as the system is in the low-excitation limit, the quantum correlations only weakly depend on the average number of photons per laser pulse[7].

[1]Department of Physics and Astronomy, Macquarie University, Sydney, New South Wales, Australia. [2]ARC Centre of Excellence for Engineered Quantum Systems, Macquarie University, Sydney, New South Wales, Australia. [3]ARC Centre for Quantum Computation and Communication Technology, School of Science, RMIT University, Melbourne, Victoria, Australia. [4]Centre de Nanosciences et de Nanotechnologies, CNRS (C2N), Universities Paris-Sud and Paris-Saclay, Palaiseau, France. [5]Univ. Lille, CNRS, UMR 8523, PhLAM - Physique des Lasers Atomes et Molécules, Lille, France. [6]Univ. Grenoble Alpes, CNRS, Grenoble INP, Institut Néel, Grenoble, France. [7]These authors contributed equally: Guillermo Muñoz-Matutano, Andrew Wood, Mattias Johnsson. *e-mail: guillermo.munozmatutano@mq.edu.au; thomas.volz@mq.edu.au

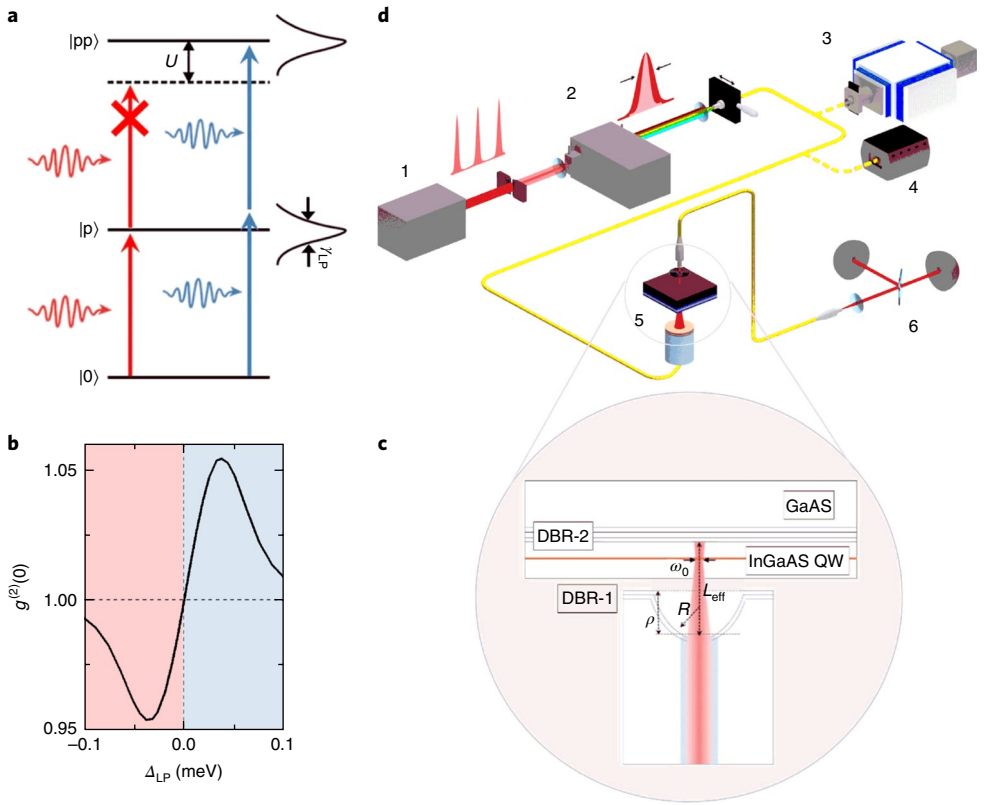

Fig. 1 | Polariton excitation ladder and experimental set-up. a, Low-energy polariton excitation spectrum. Polariton–polariton interactions shift the two-polariton state to higher energies. If the shift U is larger than the polariton linewidth γ_{LP}, polariton blockade occurs: a photon resonant with (or slightly red-detuned from) the transition from the ground state to the one-polariton state will generate a polariton, but a second photon of the same colour cannot excite the system further. It gets blocked by the first photon. For blue-detuned photons, the chance of two photons entering the system simultaneously is enhanced. **b**, As a result, photons are expected to exhibit antibunching for red detuning and bunching for blue detuning, resulting in a characteristic shape of the autocorrelation function $g^{(2)}(0)$ around the polariton resonance ($\Delta_{LP}=0$) The curve in **b** was obtained using a master equation approach and assuming realistic parameters of $\hbar\omega_{NL}\simeq 18\,\mu$eV, $\Delta=0.07$ meV, 0.7 photons per laser pulse, a cavity lifetime of 16 ps and an exciton lifetime of 10 ps. The value of $g^{(2)}(0)$ was integrated over all possible coincidence pairs as described in Supplementary Section 1. **c**, The basic fibre-cavity layout consisting of the fibre tip with dielectric Bragg reflectors (DBR-1), the GaAs cavity spacer layer and the InGaAs QW on top of a stack of alternating layers of AlAs/GaAs (DBR-2). The cavity parameters are the fibre curvature radius (R), the mirror depth (ρ), the effective cavity length (L_{eff}) and cavity mode waist (ω_0). **d**, Experimental set-up. The key ingredients for the experiment are the resonant pulsed excitation (1), laser pulse shaping (2), laser pulse monitoring with a streak camera (3), wavelength read-out using a wavemeter (4), the fibre-cavity microscope at 4 K (5) and the standard free-space Hanbury Brown and Twiss interferometer for correlation measurements (6).

The design of our fibre microcavity is shown in Fig. 1c. We use a fibre-cavity mirror with a small radius of curvature ($R=13\,\mu$m), resulting in a mode waist at the position of the quantum well (QW) of $w_0=1.17\,\mu$m (see Supplementary Section 6). This purely optical polariton confinement does not affect the polariton lifetime in contrast to other polariton confinement techniques available. In our fibre cavity we achieve lifetimes between 20 ps and 40 ps, depending on the cavity detuning $\Delta=E_c-E_x$, where E_c (E_x) is the bare cavity (exciton) energy. The excitonic fraction of the microcavity polaritons is provided by a single $In_{0.04}Ga_{0.96}As$ QW placed at the antinode of the cavity.

Figure 1d shows the main features of the experimental set-up: the pulses from a mode-locked Ti:sapphire laser are spectrally narrowed down to match the polariton lifetime, and to prevent excitation of the neighbouring polarization-split mode, labelled π_Y further on (see Supplementary Section 3). The laser pulses are injected at the other end of the mirror fibre and tuned across the polariton resonance. The transmitted light is then collected by a lens and sent through a second fibre to a Hanbury Brown and Twiss interferometer, from which a two-photon coincidence histogram is recorded and the autocorrelation function $g^{(2)}(0)$ is inferred. In the ideal case, when polariton–polariton interactions are significant, the theory predicts a characteristic dependence of $g^{(2)}(0,\Delta_{LP})$, the autocorrelation function versus the laser detuning Δ_{LP}, which is displayed in Fig. 1b for realistic values of the polariton–polariton interactions.

Before recording photon correlations, we first characterize the polariton modes in the system. Figure 2a displays a low-temperature polariton photoluminescence map as a function of cavity length, obtained under non-resonant excitation (at $E_L=1.55$ eV). As the length of the cavity changes, the energy of the fundamental mode of the cavity is swept across the excitonic transition. At resonance between the cavity and exciton, a characteristic anticrossing is observed with a vacuum Rabi splitting of $2\hbar\Omega_R=3$ meV, indicating the strong coupling regime, and thus well-defined upper polariton (UP) and lower polariton (LP) states. The UP state is subject to rapid non-radiative decay. We therefore focus on the LP mode.

Ideally, correlation measurements should be carried out for strong blue detuning of the cavity mode when the LP has strong excitonic character. However, the number of photons transmitted through the system is found to go down significantly as we blue-detune the cavity from the exciton resonance. The loss in photon number is stronger than what we expect from the coupled oscillator

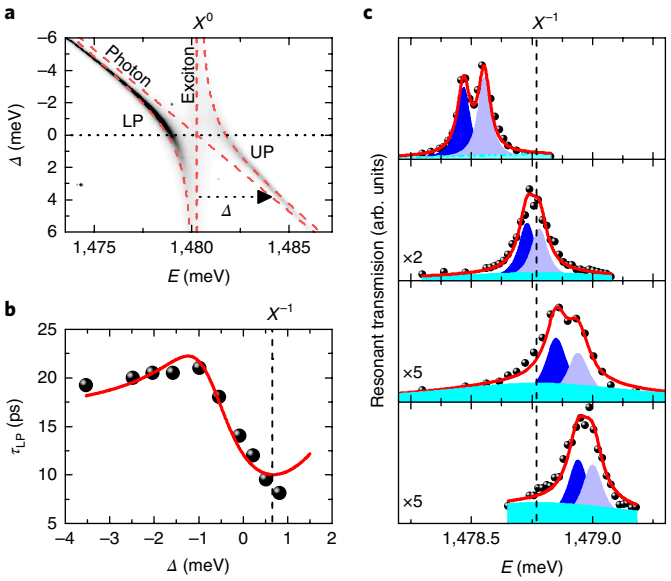

Fig. 2 | Anticrossing of the polariton states and lifetimes. a, Photoluminescence map under near-resonant excitation at 1.55 eV, showing the anticrossing of the bare exciton and the cavity mode forming lower (LP) and upper (UP) polariton dressed states near resonance ($\Delta \approx 0$). The dashed lines correspond to a fit based on a two-coupled oscillator model, yielding a Rabi vacuum splitting of $2\hbar\Omega_R = 3$ meV. **b**, Experimentally measured LP lifetime versus Δ (black dots) and best fit to a two-coupled-oscillator model when including polariton losses by elastic scattering (red line). The main mechanism of LP losses is governed by elastic scattering with negative trions X^{-1}, at a rate of $\simeq$0.1 scattering events per picosecond at $E_{LP} = E_{X^{-1}} \simeq 1.47877$ meV. **c**, Resonant transmission as a function of laser detuning for four different Δ values of 0.07, 0.52, 0.83 and 1.05 meV. As Δ increases, the polarization-split polariton doublet moves across the trion resonance, and the photonic fraction and hence the total transmission signal decrease. A fit involving three Lorentzians (two cross-polarized polariton modes and the trion resonance) best describes the data.

model and is due to additional excitonic loss channels in the system. In particular, we identified an additional excitonic feature about 1.2 meV to the red side of the excitonic transition when carrying out off-resonant photoluminescence measurements with a photon excitation energy of $E_L = 1.50$ eV, just below the GaAs-barrier bandgap (see Supplementary Section 4). In agreement with the literature, we attribute this peak to the negatively charged trion resonance (X^{-1})[19]. Its presence greatly reduces the polariton lifetime once the cavity is on the blue side of the QW resonance. Figure 2b displays measured lifetimes as a function of cavity-exciton detuning. This graph helps us to determine the best pulse parameters for resonantly probing the polariton system (see Supplementary Information). In addition to the reduced lifetime, the trion resonance adds noise to the correlation measurements as we will show.

Another effect relevant for our correlation measurements is the splitting of the fundamental transverse cavity mode into two linearly cross-polarized modes due to residual birefringence in GaAs[20] and micropillars[21]. We characterized this feature by carrying out resonant transmission measurements for different detunings Δ, as shown in Fig. 2c. The two peaks correspond to the two polarization-split polariton modes π_X and π_Y, along with the trion background that is also discernible.

Having these two effects in mind, we carried out a first set of correlation measurements for three different cavity-exciton detunings Δ. At each Δ, we took data for five different laser detunings (Δ_{LP}), where $\Delta_{LP} = 0$ corresponds to the laser at resonance with the π_X polariton mode. While we tried to excite predominantly the π_X mode, the polarization was not monitored and actively corrected during correlation measurements. However, in an independent characterization measurement we found the polarization to be stable over hours. For each pair (Δ_{LP}, Δ), a raw coincidence trace like the one shown in Fig. 3d is obtained. This figure is a zoomed-in version of the full-scale trace shown in Supplementary Fig. 5. The arrow in Fig. 3d indicates the position of the zero-delay peak that contains the quantum correlations of the system and that is used to extract $g^{(2)}(0)$. The immediate neighbouring peaks are neglected in the analysis since they exhibit bunching due to the avalanche photodiode (APD) crosstalk[22]. All other peaks are far apart in time ($n \times 13$ ns) and constitute a reference of purely uncorrelated detection events. From raw traces such as this one, $g^{(2)}(0)$ as well as its 1σ confidence interval is extracted (see Supplementary Section 5). The result of this analysis for the 15 pairs (Δ_{LP}, Δ) is shown in Fig. 3a–c.

The experimental plots of $g^{(2)}(0, \Delta_{LP})$ obtained in this way exhibit substantial deviations from the uncorrelated baseline $g^{(2)}(0) = 1$. Consistently, and in line with the theoretical expectation, $g^{(2)}(0, \Delta_{LP})$ is mostly smaller than 1 for negative Δ_{LP} and larger than 1 for positive Δ_{LP}. These deviations from 1 reflect the presence of additional quantum correlations generated by transmission through the fibre-cavity polariton system. However, for some of the data points (in particular Fig. 3c), the deviations are not in line with theoretical expectations from the single-mode polariton blockade model.

To get a quantitative understanding of our data, we developed a numerical simulation based on a master equation approach[7] taking into account our experimental parameters, the pulsed nature of the excitation and the experimental integration over all possible correlation times (see Supplementary Section 1). Our model does not include the effects of the trion resonance or the neighbouring polariton mode π_Y as this would require new theoretical developments beyond the scope of this paper. Instead, to make sense of the comparison between experiment and theory, we determine the range of validity of the model. To do so, we define a quantity $\widetilde{T}(\Delta_{LP})$ (see Supplementary Section 4) that quantifies the fraction of laser light transmitted by the π_X polariton mode alone. It estimates the amount of perturbation this mode is subject to for a given Δ_{LP}, due to its spectral overlap with the other perturbing transitions. The smaller $\widetilde{T}$, the more the π_X polariton mode is perturbed, and the more the experiment is expected to depart from the single-mode theoretical expectation.

The resulting $\widetilde{T}(\Delta_{LP})$ is shown as middle panels in Figs. 3a–c and 4a. In addition, it is also underlaid as a colour map with the measured $g^{(2)}(0)$ data points in the lowest panels of Figs. 3a–c and 4a. Interestingly, data points lying in high values of $\widetilde{T}$ (light areas) exhibit a very good quantitative agreement with the theoretical expectation.

This is the case, for example, of most points close to resonance ($\Delta_{LP} \simeq 0$), where a trend towards antibunching is visible. The point labelled (i) in Fig. 3c is particularly interesting as it benefits from a good $\widetilde{T}$, a large excitonic fraction and $\Delta_{LP} \approx 0$, a situation in favour of the strongest antibunching among all data points. Despite this, the measurement uncertainty remains rather large and the perturbation is non-zero ($\widetilde{T} = 0.65$), so that it is hard to infer the actual value of $g^{(2)}(0)$ we would find in an ideal measurement in the absence of perturbation from the trion.

Points lying in low-$\widetilde{T}$ areas on average exhibit an excess of bunching as compared to the theory. This is particularly clear for the three leftmost points in Fig. 3c, for which the perturbation is mostly due to interaction with the trion resonance. This trend is actually expected, as coupling with the trion transition, and in particular re-emission through the polariton mode, will generate classical noise of thermal origin (mediated by trion–phonon or trion-free charge interaction). When the perturbation comes from the neighbouring cross-polarized polariton mode, the influence on $g^{(2)}(0)$ seems

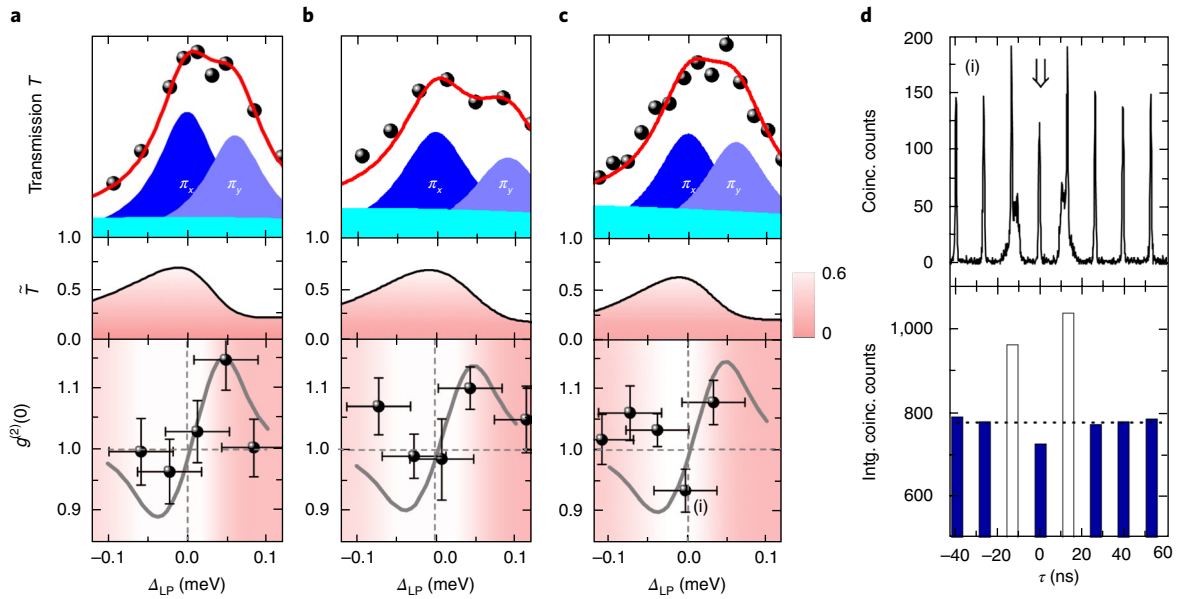

Fig. 3 | Quantum-correlated photons with cavity-exciton detuning. a–c, Photon autocorrelation data $g^{(2)}(0)$ for three different cavity-exciton detunings $\Delta = 0.14$ (**a**), 0.83 (**b**) and 1.11 meV (**c**). At each Δ, we measured $g^{(2)}(0)$ for five different laser detunings, Δ_{LP}. Each subfigure contains three subpanels, with the top panel showing the corresponding resonant laser scan. The bottom panel displays the corresponding correlation data (black dots) along with the calculation from the single-mode theory (two lines corresponding to the upper and lower bound of the interaction strength). The middle panel contains a plot of the transmission fraction $\widetilde{T}$. This parameter gives an indication of the perturbation of the mode of interest, π_x, through the presence of the orthogonally polarized polariton mode π_y and the trion resonance. Both are expected to lead to a significant deviation of the measured $g^{(2)}(0)$ from the single-mode theory. Hence, only regions with large $\widetilde{T}$ are expected to give correlation data that are close to the expected theory values. In **c**, only the data point (i) around zero detuning Δ_{LP} shows negligible influence from π_y and the trion resonance. It exhibits antibunching around $g^{(2)}(0) = 0.93 \pm 0.04$. **d**. The dip at zero time delay is clearly visible both in the raw correlation trace and the integrated coincidences plot. The experimental uncertainty in $g^{(2)}(0)$ was determined from the standard deviation in the total counts of all the uncorrelated peaks; full details can be found in Supplementary Section 5.

less dramatic (compare, for example, the two rightmost points in Fig. 3a,b). This is reasonable as a polariton mode is much shorter lived and much less coupled to thermal noise mediated by phonons or free charges. In this case, the polariton–polariton correlations are largely lost due to a loss of the single-mode character of the polariton modes and an effective loss of the interaction strength. We thus see that our entire dataset can be qualitatively, and to some extent quantitatively, explained by polariton-interaction-mediated correlations that are significantly altered by the presence of unwanted transitions, namely, the trion resonance and the cross-polarized polariton mode.

For the final measurement, we attempted to optimize the microcavity parameters such that $\widetilde{T}$ was as large as possible over a broad window of Δ_{LP}. This situation is met for $\Delta = 0.07$ meV, where the polarization split polariton modes are well separated, and the trion resonance lies far away on the blue side of the polariton mode. The results are shown in Fig. 4a (bottom panel), together with the transmission spectrum (top panel) and $\widetilde{T}(\Delta_{LP})$ (middle panel). These data are consistent with our previous analysis: the rightmost points that approach the trion resonance as well as the π_Y polariton mode exhibit a slight excess of bunching (which lies within the error bars). The left-side points, which are very well protected from the sources of perturbation, are well in line with the theoretical prediction. The leftmost point being strongly detuned from the polariton mode has weak transmission and thus suffers from a low count number, which is reflected by its extremely large error bar. The raw coincidence traces for the points labelled (i) ($g^{(2)}(0) = 0.98 \pm 0.04$) and (ii) ($g^{(2)}(0) = 1.06 \pm 0.04$) are shown in Fig. 4b as an illustration of the kind of raw correlation traces obtained for a high photon number.

Owing to a better signal-to-noise ratio, we took advantage of this dataset to determine the strength of the polariton–polariton nonlinearity by comparing it to our model. The best fit is obtained for a confinement-enhanced exciton–exciton interaction constant $\hbar\omega_{NL} = 0.018 \pm 0.010$ meV, corresponding to a polariton–polariton nonlinearity $\hbar g_0 = 0.020 \pm 0.011$ meV μm^2 (see Supplementary Section 2). The calculated $g^{(2)}(0, \Delta_{LP})$ for this value is shown as the solid line (orange) in Fig. 4a (bottom panel). For this fitting, we excluded the two rightmost points at large positive Δ_{LP} as they have low $\widetilde{T}$ and are not expected to fit the theory. The confidence of this value is illustrated by the plot in Fig. 4c showing the coefficient of determination $R^2(\hbar g)$ of the theoretical fit to our data. The polariton–polariton nonlinearity extracted from our measurements is in good agreement with previously reported values[18,23,24] and with the value in the similar experiment by Delteil et al.[25].

Together with the results of Delteil et al., as well as an additional set of measurements that we have carried out on a second cavity (see Supplementary Section 7), our work demonstrates the emergence of quantum correlations from cavity polaritons. It is important to note that no evidence of trion formation and trion-induced polariton losses was found in Delteil et al. A difference in unintentional residual free charges is indeed expected in these independent experiments, in which both microcavities have been fabricated by different groups, in different facilities. Hence, from a materials perspective, the two works are complementary and provide valuable insight into the underlying material physics.

In summary, our work demonstrates two key facts highlighting the potential of polaritons for the manipulation of the quantum statistics of light: in our microcavity design, polariton–polariton interactions are strong enough to modify the photon statistics of a weak light beam; and to optimize this effect, not only the photonic mode needs to be further engineered to provide stronger optical confinement and possibly even stronger polarization splitting for clean mode separation. In addition, the solid-state environment in which a polariton mode lives has to be taken into account: unwanted

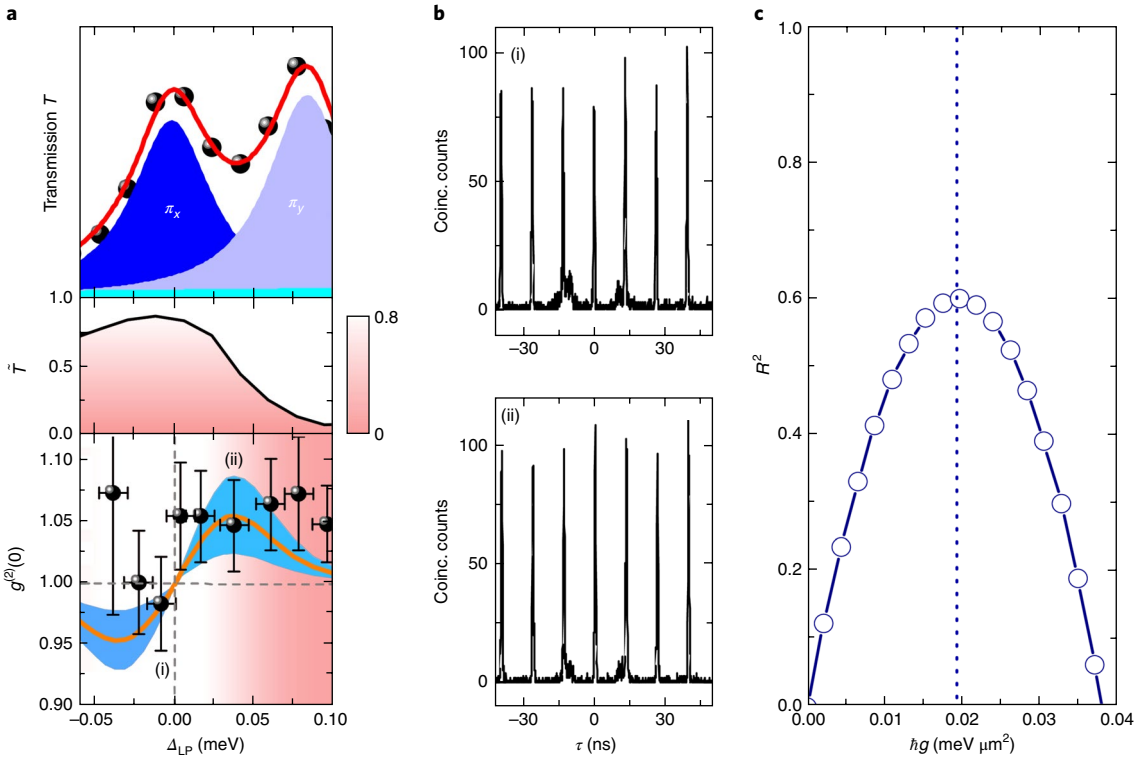

Fig. 4 | Polariton–polariton interaction constant. a, Correlation data near cavity-exciton resonance. The top panel contains the corresponding resonant transmission laser scan while the middle panel shows the calculated transmission fraction $\tilde{T}$. The bottom panel displays $g^{(2)}(0)$ as a function of laser detuning Δ_{LP} from the position of the LP π_x resonance for a cavity-exciton detuning of $\Delta = 0.07$ meV. The black dots indicate measured values while the solid orange line is a theoretical prediction based on the polariton-polariton interaction constant extracted in panel **c**. The blue shaded region indicates how the model prediction changes when varying the nonlinearity. Except for the two rightmost data points, which are heavily influenced by the π_y mode, all data points are from almost pure π_x-mode photons. The experimental uncertainty in $g^{(2)}(0)$ was determined from the standard deviation in the total counts of all the uncorrelated peaks; full details can be found in Supplementary Section 5. **b**, Example raw correlation traces from the two points (i) and (ii) in **a**. **c**, Coefficient of determination R^2 of the data fit with the theoretical model versus the interaction parameter $\hbar g$. The most likely value is $\hbar g_0 = 0.020 \pm 0.011$ meV μm^2.

perturbing transitions, such as the trion resonance, need to be suppressed. If these issues can be addressed, it will be possible to move significantly into the polariton blockade regime. Once this goal is realized, an immediate follow-up would be the realization of strongly driven, dissipative small arrays of a few nonlinear cavities, with the potential of demonstrating spin frustration[26] and fermionization[27] in a completely new parameter regime. Further in the future, polariton-based high-repetition-rate single-photon emitters[7], Fock-state optical switchers and all-optical quantum gates[28], and light-based two-dimensional driven dissipative quantum simulators[29] might be tangible.

Online content

Any methods, additional references, Nature Research reporting summaries, source data, statements of data availability and associated accession codes are available at https://doi.org/10.1038/s41563-019-0281-z.

Received: 14 December 2017; Accepted: 21 December 2018;
Published online: 18 February 2019

References

1. Carusotto, I. & Ciuti, C. Quantum fluids of light. *Rev. Mod. Phys.* **85**, 299–366 (2013).
2. Berloff, N. G. et al. Realizing the classical XY Hamiltonian in polariton simulators. *Nat. Mater.* **16**, 1120–1126 (2017).
3. Jacqmin, T. et al. Direct observation of Dirac cones and a flatband in a honeycomb lattice for polaritons. *Phys. Rev. Lett.* **112**, 116402 (2014).
4. Baboux, F. et al. Bosonic condensation and disorder-induced localization in a flat band. *Phys. Rev. Lett.* **116**, 066402 (2016).
5. Dagvadorj, G. et al. Nonequilibrium phase transition in a two-dimensional driven open quantum system. *Phys. Rev. X* **5**, 041028 (2015).
6. Klembt, S., Stepanov, P., Klein, T., Minguzzi, A. & Richard, M. Thermal decoherence of a nonequilibrium polariton quantum fluid. *Phys. Rev. Lett.* **120**, 035301 (2018).
7. Verger, A., Ciuti, C. & Carusotto, I. Polariton quantum blockade in a photonic dot. *Phys. Rev. B* **73**, 193306 (2006).
8. Boulier, T. et al. Polariton-generated intensity squeezing in semiconductor micropillars. *Nat. Commun.* **5**, 3260 (2014).
9. Cuevas, Á. et al. First observation of the quantized exciton-polariton field and effect of interactions on a single polariton. *Sci. Adv.* **4**, eaao6814 (2018).
10. Savasta, S., Stefano, O. D., Savona, V. & Langbein, W. Quantum complementarity of microcavity polaritons. *Phys. Rev. Lett.* **94**, 246401 (2005).
11. Amo, A. et al. Exciton-polariton spin switches. *Nat. Photon.* **4**, 361–366 (2010).
12. Birnbaum, K. M. et al. Photon blockade in an optical cavity with one trapped atom. *Nature* **436**, 87–90 (2005).
13. Lang, C. et al. Observation of resonant photon blockade at microwave frequencies using correlation function measurements. *Phys. Rev. Lett.* **106**, 243601 (2011).
14. Liebisch, T. C., Reinhard, A., Berman, P. R. & Raithel, G. Atom counting statistics in ensembles of interacting Rydberg atoms. *Phys. Rev. Lett.* **95**, 253002 (2005).
15. Jia, N. et al. A strongly interacting polaritonic quantum dot. *Nat. Phys.* **14**, 550–554 (2018).
16. Faraon, A. et al. Coherent generation of non-classical light on a chip via photon-induced tunnelling and blockade. *Nat. Phys.* **4**, 859–863 (2008).
17. Reinhard, A. et al. Strongly correlated photons on a chip. *Nat. Photon.* **6**, 93–96 (2012).
18. Walker, P. M. et al. Dark solitons in high velocity waveguide polariton fluids. *Phys. Rev. Lett.* **119**, 097403 (2017).

19. Deveaud, B. et al. Excitonic effects in the luminescence of quantum wells. *Chem. Phys.* **318**, 104–117 (2005).
20. Besga, B. et al. Polariton boxes in a tunable fiber cavity. *Phys. Rev. Appl.* **3**, 014008 (2015).
21. Reitzenstein, S. et al. AlAs/GaAs micropillar cavities with quality factors exceeding 150.000. *Appl. Phys. Lett.* **90**, 251109 (2007).
22. Wood, A., Vidal, X., Muñoz-Matutano, G. & Volz, T. Non-invasive zero delay calibration of Hanbury Brown and Twiss interferometer. *Measurement* https://doi.org/10.1016/j.measurement.2019.01.079 (2019).
23. Amo, A. et al. Superfluidity of polaritons in semiconductor microcavities. *Nat. Phys.* **5**, 805–810 (2009).
24. Ferrier, L. et al. Interactions in confined polariton condensates. *Phys. Rev. Lett.* **106**, 126401 (2011).
25. Delteil, A. et al. Towards polariton blockade of confined exciton-polaritons. *Nat. Mater.* https://doi.org/10.1038/s41563-019-0282-y (2019).
26. Casteels, W., Rota, R., Storme, F. & Ciuti, C. Probing photon correlations in the dark sites of geometrically frustrated cavity lattices. *Phys. Rev. A* **93**, 043833 (2016).
27. Carusotto, I. et al. Fermionized photons in an array of driven dissipative nonlinear cavities. *Phys. Rev. Lett.* **103**, 033601 (2009).
28. Miller, D. A. B. Are optical transistors the logical next step?. *Nat. Photon.* **4**, 3–5 (2010).
29. Noh, C. & Angelakis, D. G. Quantum simulations and many-body physics with light. *Rep. Prog. Phys.* **80**, 016401 (2017).

Acknowledgements

We thank S. Martin and D. Taylor from the Commonwealth Scientific and Industrial Research Organisation (Lindfield – New South Wales) for their technical support. This work was funded by the Australian Research Council Centre of Excellence for Engineered Quantum Systems (CE110001013 and CE170100009). A.L., J.B., A.A. and M.R. acknowledge support from the French Agence National de la Recherche (contract no. ANR-16-CE30-0021).

Author contributions

G.M.-M. and A.W. carried out the spectroscopy and photon correlation experiments and analysed the data. M.J., with the help of B.Q.B., implemented the master equation model and contributed to the analysis of the data. G.M.-M., A.W. and M.J. have equally contributed to this research. X.V. built the spectroscopy set-up. A.R. and B.B. built the cavity microscope and designed the laser machining system for making the fibre cavities. A.L., J.B. and A.A. provided the QW sample and discussed the underlying polariton physics. G.N. carried out the finite-elements simulation of the cavity mode. M.R. and T.V. conceived the central idea of the work and related experiments, supervised the experimental work and contributed to discussions. The manuscript was written by G.M.-M., M.J., M.R. and T.V. with varying contributions from all other authors.

Competing interests

The authors declare no competing interests.

Additional information

Supplementary information is available for this paper at https://doi.org/10.1038/s41563-019-0281-z.

Reprints and permissions information is available at www.nature.com/reprints.

Correspondence and requests for materials should be addressed to G.M. or T.V.

Publisher's note: Springer Nature remains neutral with regard to jurisdictional claims in published maps and institutional affiliations.

Methods

Excitation method and detector choice. To be able to detect the interaction-induced quantum correlations that are expected to deviate from $g^{(2)}(0)=1$ at the few percent level, the experimental measurement technique has to be carefully chosen. The combination of continuous-wave laser excitation and a readily available detection set-up based on state-of-the-art APDs is not feasible due to the very limited overall time resolution of ~65 ps[30] combined with low quantum efficiency. Using a streak camera with 2 ps time resolution and the ability to record photon coincidences would be possible, but its very low quantum efficiency at 835 nm does not allow for working in the low-excitation regime, in which events involving more than two polaritons are strongly suppressed. We therefore resort to pulsed excitation and slow APDs with a high quantum efficiency of 55% at 835 nm. This method was used successfully in the past for the demonstration of photon blockade in a quantum-dot photonic-crystal cavity with similarly short decay times[16,17].

Fibre-cavity microscope and sample. The home-built fibre cavity set-up is sitting in a liquid-helium Dewar at 4 K. The cavity itself consists of a curved fibre-based top mirror with a highly reflective dielectric Bragg coating (Laseroptik GmbH) with a designed finesse of a few tens of thousands. Its small curvature radius ($R=13\,\mu$m) ensures tight mode confinement. The depth of the curved mirror is $\rho=1.3\,\mu$m. The second cavity mirror is a molecular beam epitaxy-grown AlAs/GaAs DBR mirror (45 pairs) with a single $In_{0.04}Ga_{0.96}As$ 10-nm-thick QW on top and embedded in two GaAs half-wavelength spacers. The sample and fibre tip are mounted on attocube positioners for controlling the lateral position and distance of the fibre tip relative to the sample. For all photon correlation measurements described here, the effective cavity length was calculated to be around 4.8 µm, taking into account the effective penetration depth into the AlAs/GaAs mirror[20] and the depth of the curved mirror (ρ). Using a finite-elements simulation of the cavity set-up, we find that the mode radius (at $1/e^2$ of the mode intensity) at the position of the QW amounts to 1.17 µm.

Resonant transmission measurements. For continuous-wave resonant transmission measurements, we use a highly stable wavelength-tunable continuous-wave Ti:sapphire laser (SolsTiS from M-Squared). The power sent into the fibre cavity is monitored carefully. The light transmitted through the fibre cavity is directed onto silicon APDs for detection (SPCM-AQRH-14 from Excelitas). Photons are counted using the correlator box PicoHarp 300 from PicoQuant. For time-resolved and pulsed resonant correlation measurements, a pulsed Ti:sapphire laser (MIRA) with 76.3 MHz repetition rate and 4 ps pulse width is used for excitation. Resonant lifetime traces are recorded on a streak camera with a temporal resolution of around 2 ps (OptoScope from Optronis GmbH). Conventional photoluminescence is excited with the continuous-wave Ti:sapphire laser, and detected on the silicon CCD (charge-coupled device; Pixis 100) attached to the monochromator with 1,500 grooves mm^{-1} grating (Acton Spectra Pro 2750).

Photon autocorrelation. Photon autocorrelation data are measured with a conventional free-space Hanbury Brown and Twiss interferometer. The two free-space silicon APDs have a quantum efficiency of ~55% at 830 nm and a time resolution of around ~350 ps. The total coincidence counts in each peak were evaluated by counting coincidences within the pulses. The experimental uncertainty in $g^{(2)}(0)$ was determined from the standard deviation in the total counts of all the uncorrelated peaks. Note that unwanted APD crosstalk[17,22] contributes to the two peaks at ±13 ns. We thus discarded them in the ensuing statistical analysis (the method to derive $g^{(2)}(0)$ is described in the Supplementary Information).

Pulse shaping. To adapt the resonant probe pulses to the measured resonant polariton lifetimes, we shape the temporal width of the intrinsic laser pulses from the MIRA laser by sending them through the monochromator. The effective numerical aperture is controlled via an iris before the entrance slit of the monochromator and determines the effective laser pulse width at the monochromator output. The pulses are then coupled into a single-mode optical fibre for delivery to the fibre cavity. The single-mode fibre at the monochromator output acts as a pinhole. The monochromator grating angle controls the centre wavelength of the laser pulse. The method provides effective tuning of the laser pulse widths between 15 and 50 ps (see Supplementary Information). The pulse shapes are monitored on the streak camera; the pulse centre wavelengths are read-out using a wavemeter from High Finesse (WSU-10).

Agreement between data and model. To have a quantitative estimation for the deviation between the model and the data, we define the so-called coefficient of determination as:

$$R^2 = 1 - \frac{\sum \left(g_i^{(2)}(0)_{\mathrm{Exp}} - g_i^{(2)}(0)_{\mathrm{Mod}}\right)^2}{\sum \left(g_i^{(2)}(0)_{\mathrm{Exp}} - 1\right)^2}$$

where $g_i^{(2)}(0)_{\mathrm{Exp}}$ denotes the measured values for $g^{(2)}(0)$, $g_i^{(2)}(0)_{\mathrm{Mod}}$ are the numerical predictions for $g^{(2)}(0)$ and the '1' in the denominator represents $g^{(2)}(0)=1$ for uncorrelated photons. R directly gives a measure for how much the data are consistent with strongly interacting polaritons versus completely uncorrelated polaritons. $R=1$ indicates a perfect match between the data and the model.

Data availability

All data presented in this work are available on request from the authors.

References

30. Hadfield, R. H. Single-photon detectors for optical quantum information applications. *Nat. Photon.* **3**, 696–705 (2009).